BUTTERWORTH HEINEMANN

Polymer Vol. 36 No. 11, pp. 2143–2152, 1995

0032-3861/95/$10.00 + 0.00

Crystalline morphology of polyamide-6 near planar surfaces

O. K. Muratoğlu
Program in Polymer Science and Technology, and Department of Material Science and Engineering, Massachusetts Institute of Technology, Cambridge, MA 02139, USA

and A. S. Argon
Department of Mechanical Engineering, Massachusetts Institute of Technology, Cambridge, MA 02139, USA

and R. E. Cohen*
Department of Chemical Engineering, Massachusetts Institute of Technology, Cambridge, MA 02139, USA
(Received 16 June 1994; revised 27 October 1994)

The crystalline morphology and the orientation in thin films of polyamide-6 crystallized on polystyrene- or ethylene–propylene–diene rubber-coated silicon substrates were analysed by transmission electron microscopy (TEM), X-ray and electron diffraction. Bright-field TEM imaging of thin films demonstrated that lamellae organize into disc-shaped crystals, or 'discoids', when the film thickness is below 0.5 μm. A model is presented for the organization of lamellae and the polyamide-6 chains in the lamellae of the discoids. In the inter-discoid regions, the films are semicrystalline and the lamellae fill the space randomly. Orientation studies by means of electron diffraction and wide-angle X-ray scattering showed that in relatively thin films (<0.5 μm) the (0 0 2) hydrogen-bonded planes are parallel to the surface of the film. This orientation gradually diminishes as the film thickness increases. The change in orientation affects the mechanical properties: under uniaxial tension, the modulus and the flow stress of the films increase with decreasing thickness, hence with increasing orientation.

(Keywords: polyamide; crystalline morphology; thin films)

INTRODUCTION

Polyamides are known to be high-strength engineering thermoplastics. Although they are ductile at room temperature, they become brittle under severe conditions such as high strain rates and/or low temperatures[1]. This is due to the low crack propagation resistance of polyamides in general[2]. Several methods are effective in modifying these materials. For instance, rubber particles within a range of particle size and rubber concentration enhance the toughness by as much as 50-fold[3,4]. Similarly, the presence of glass fibres can improve both the toughness and the fatigue and creep resistances[5,6]. Composites of polyamide-6 with poly(*p*-phenylene terephthalamide) (PPTA) fibres have excellent mechanical properties[7]. The presence of a modifying inclusion influences the crystallization behaviour of the matrix. Second-phase particles that are crystalline at the crystallization temperature of the matrix often act as heterogeneous nucleation sites, resulting in epitaxial growth of the polyamide matrix. For instance, polyamide-6 crystallizes epitaxially at a PPTA fibre interface with the chain direction almost perpendicular (inclined 84°) to the fibre axis[8]. In a polyamide-6/clay hybrid, epitaxy results in the preferred orientation of the γ-(0 2 0) hydrogen-bonded planes parallel to the montmorillonite inclusion interface[9].

In most cases, this influence of the interface vanishes when the substrate is amorphous. However, interface effects have been observed in several systems where an amorphous substrate induces an artificial epitaxy in the crystallizing matrix[10–14]. For instance, Andrews[12] demonstrated that *cis*-polyisoprene thin films on a water substrate crystallize with a preferred orientation of chain axis perpendicular to the film plane. The films displayed no preferred azimuthal orientation. When the same films are crystallized under uniaxial strain, the chain axis acquires a new orientation parallel to the film plane[11]. Similarly, Keller[13] and Scott[14] studied the orientation in thin films of polyamide-6,6 and -6,10 prepared by shearing a solution on a hot glass plate. The films were not annealed following the evaporation of the solvent, hence they carried along the orientation induced by shearing. Both studies showed that crystallization in polyamide thin films results in the orientation of the hydrogen-bonded planes parallel to the film plane. The present paper investigates the effect of film thickness on the

* To whom correspondence should be addressed

orientation and crystalline morphology in thin films of polyamide-6 melt crystallized on a rubbery substrate. The results of this orientation study on thin films are consistent with the findings of Keller[13] and Scott[14]. In thicker films the orientation approaches a random texture. In thin films the preferred orientation arises from the overlapping effect of the interfaces.

EXPERIMENTAL

Thin films

Thin films of polyamide-6 were prepared by spin coating on a silicon substrate. The spinning rate and the concentration of the solutions, given in *Table 1*, were chosen to obtain films with thicknesses ranging from 0.15 to 2.25 μm. *Figure 1* shows a schematic rendering of the multilayer films made in the spin coating process. The substrate was a silicon wafer on top of which a layer of polystyrene (PS) or ethylene–propylene–diene rubber (EPDR) was deposited from a solution of toluene or hot xylene respectively. The polyamide-6 film was spin coated from a trifluoroethanol (TFEtOH) solution as a second layer. Finally, a top layer of PS or EPDR was added to sandwich the thin film of polyamide. A profilometer, Dektak 8000, was used to measure the thickness of each layer. The thickness of the polyamide-6 layer did not depend on whether it was spin coated on EPDR or PS. After the thin film preparation, each sample was subjected to a thermal treatment to remove the orientation induced through the spinning process by melting and recrystallizing the polyamide-6 layer. A brass vacuum chamber in an oil bath was used to melt the films at 225°C for 20 min. Following the melting process, the vacuum chamber was rapidly immersed in a second oil bath, which was kept at various annealing temperatures (170–210°C). The films were subjected to such isothermal crystallization excursions for 20 min.

PS and EPDR were used interchangeably as the contact surface for polyamide films. During the thermal treatment, the temperature was always above the glass transition temperature of PS. Therefore, the substrate for polyamide was always in a rubbery state during the crystallization of the polyamide-6 film.

Table 1 Thickness of polyamide-6 thin films

Concentration (wt%)	Substrate spinning rate (rpm)	Thickness (μm)
3	4000	0.15 ± 5.0%
3	3000	0.20 ± 6.0%
5	3000	0.60 ± 10%
7	3000	1.00 + 6.0%
10	3000	2.25 ± 7.0%

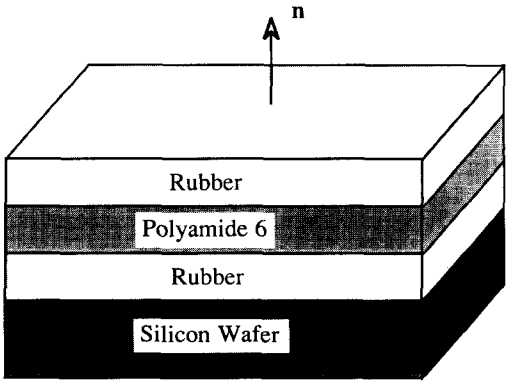

Figure 1 Schematic of the spin-coated layers of rubber and polyamide-6 on a silicon wafer. The top and bottom rubber layers are coated from a solution of hot xylene and the sandwiched polyamide-6 layer is spin coated from a solution of trifluoroethanol. Here ***n*** is the normal to the film plane

Transmission electron microscopy

For electron microscopy studies the films had to be placed on a copper grid; however, after the thermal treatment, the films adhere strongly to the substrate and it is impossible to remove the polyamide layer. Therefore, it was necessary to dissolve the PS or EPDR film. Since the former is readily soluble in toluene, polyamide films sandwiched between polystyrene layers were preferred for microscopy. These films were soaked in toluene to dissolve the polystyrene layers after the thermal treatment. Subsequently, the free-standing polyamide-6 films were transferred to copper grids, which were further exposed to toluene vapours to dissolve any remaining polystyrene. No staining was necessary to view the crystals; mass thickness contrast induced by radiation damage provided the contrast for bright-field imaging at an accelerating voltage of 200 kV with a JEOL 200CX transmission electron microscope. The orientation and the crystal structure of the films were qualitatively determined by electron diffraction at an accelerating voltage of 100 kV under normal incidence (sample perpendicular to electron beam) and at various tilt angles. The electron diffraction patterns were internally calibrated with a standard of cubic thallous chloride (TlCl) of known d spacings.

X-ray diffraction

The crystalline orientation in the thin films was qualitatively determined from $2\theta/\theta$ scans and partial pole figure measurements. These experiments were performed on a horizontal goniometer and a pole figure attachment using a Rigaku RU200 rotating-anode X-ray generator (Cu Kα radiation) with a point source. An accelerating voltage of 50 kV and an intensity of 60 mA was used. Following thermal treatment, the thin films were spun at 3000 rpm while washing with toluene to remove the top PS layer. When the polyamide film was sandwiched between EPDR films, the top layer was spin dissolved by washing with hot xylene (90°C). After the films were spin-dried, X-ray measurements in reflection mode were performed while the films were still lying flat on the silicon substrate. For transmission mode, free-standing films were prepared by selectively dissolving the PS layers in toluene.

The films were too thin (0.15–5.00 μm) and had a signal-to-noise ratio that was too low for a reliable X-ray analysis in the transmission mode. Diffraction peaks that were just discernible above the background noise in reflection mode could not be resolved in transmission mode. Consequently, a conventional pole figure measurement was incapable of furnishing information on the orientation of the crystals. Therefore, partial pole

figure measurements were used, where $2\theta/\theta$ scans at various δ angles were recorded (see *Figure 2*) to calculate the integrated intensity of the strong (0 0 2) diffraction peak from the hydrogen-bonded sheets. The thin film was mounted on a pole figure goniometer, which can rotate independently around three mutually orthogonal axes. For this method, only δ rotations around the horizontal axis were used to determine the crystalline orientation. Standard $2\theta/\theta$ scans from 22° to 26° were performed at small steps (5–10°) of δ, which was varied from 0° to 75°, the upper limit of the pole figure attachment. For these measurements the slit system was chosen to provide a 0.3° divergent incident beam.

Mechanical testing

The thin films were subjected to uniaxial tension in an Instron 4200 testing machine using a special load cell with a maximum capacity of only 2.5 N. For these experiments thin films of uniform thickness were prepared by spin coating, followed by a procedure of detaching them from substrates after the thermal treatment. The films were spin coated on a square silicon wafer ($3 \times 3\,cm^2$). Following the thermal treatment, the films and substrate were placed in liquid nitrogen and rectangular pieces were cryofractured from the centre region of uniform thickness. The cryofracturing is rather simple, as cracks follow straight paths along the cleavage planes of the single-crystal wafer of the chosen orientation, and results in perfectly uniform rectangular-shaped samples. Since the films are very fragile and adhere strongly to the substrate after annealing, it is impossible to remove them directly from the silicon wafer. The first PS layer was very useful in helping to detach the polyamide-6 film from the substrate following the thermal treatment. *Figure 3* shows schematically the sample preparation method for the uniaxial tensile test. The annealed films are directly immersed in a toluene bath to dissolve the PS layers. After 10 min the film, still lying on top of the wafer, is taken out of the bath and two pieces of adhesive tape are attached to two opposing edges. By slowly lifting the adhesive tapes, the films are separated from the substrate. Subsequently, the films are mounted on cardboard frames and subjected to toluene vapours to remove any remaining PS. For the uniaxial tensile test, the cardboard frames were mounted on the Instron machine. Before applying the load, the frames were cut and the films were strained at room temperature. A cross-head speed of $5\,mm\,min^{-1}$ was used, which, for the range of gauge lengths of specimens tested, corresponded to an initial strain rate ranging from 6×10^{-3} to $9 \times 10^{-3}\,s^{-1}$.

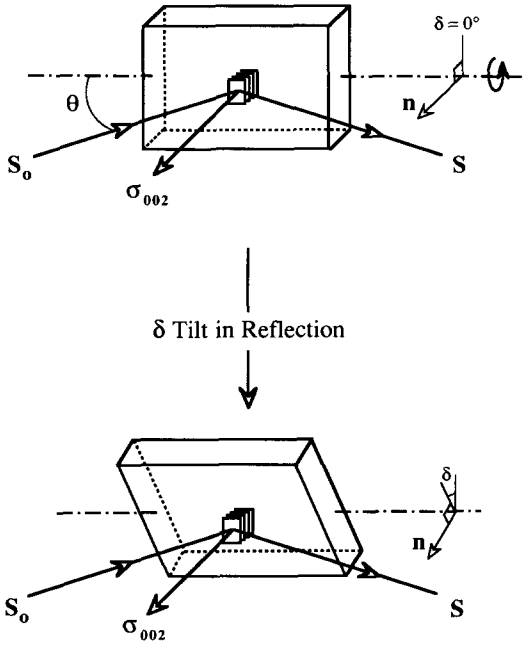

Figure 2 Schematic of the partial pole figure measurement where the sample is mounted on a goniometer and $2\theta/\theta$ scans are carried out at various values of tilt angle δ; σ_{002} represents the reciprocal lattice vector that would be normal to (0 0 2) planes; S_0 and S are the incident and diffracted beam vectors

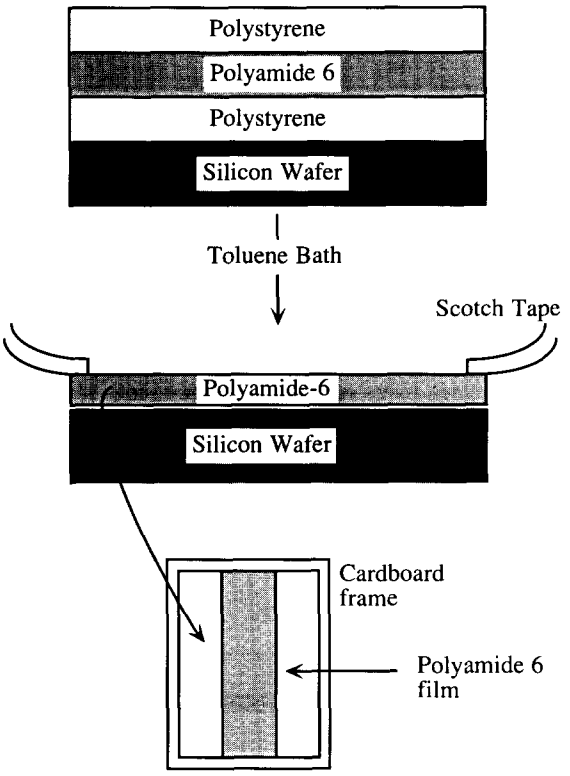

Figure 3 Detaching the polyamide-6 film from the substrate after the thermal treatment: the films are shown schematically on the silicon wafer. The polystyrene layers are dissolved in a toluene bath and the polyamide-6 film is removed by means of a pair of adhesive tape strips. The free-standing film is then mounted on a cardboard frame

RESULTS

Thin films of polyamide-6 are transparent to electrons in TEM in the thickness range of 0.10 to 2.00 μm. *Figures 4* and *5* are two electron micrographs from an unstrained thin film of 0.15 μm thickness. During TEM exposure, the crystallites first appear as unresolved black shadows. In 3–4 s, however, the shadows develop into the images seen in *Figures 4* and *5*. In these images the dark figures define the crystalline lamellae, in disc-shaped aggregates to be called 'discoids'. Besides these discoids of crystallites (*Figure 4*), the remaining morphology

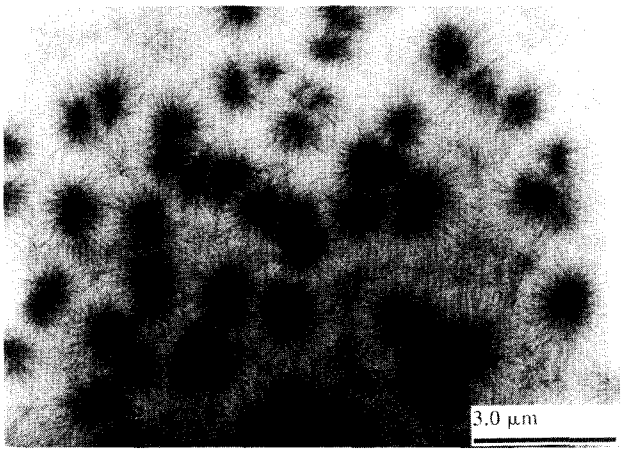

Figure 4 TEM micrograph of discoids in a 0.15 μm thick film crystallized between two polystyrene layers at 180 C for 1 h, following a melting treatment at 225 C for 1 h. The film is not stained, and the electron beam destroys the crystals, giving a mass thickness contrast

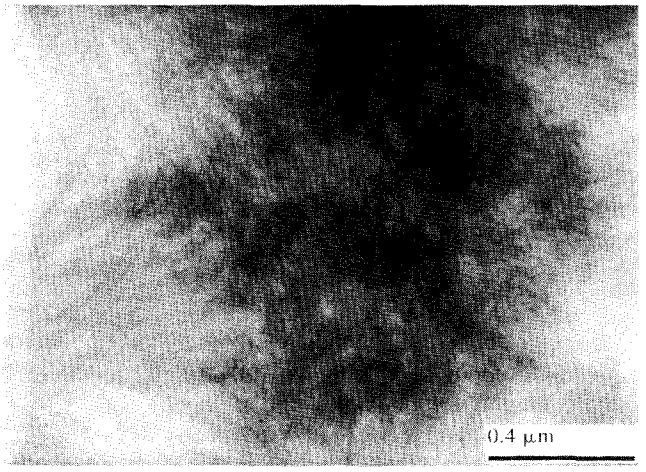

Figure 5 TEM micrograph of an inter-discoid region in a thin film of 0.15 μm polyamide-6 crystallized between two polystyrene layers at 180 C for 1 h, following a melting treatment at 225 C for 1 h

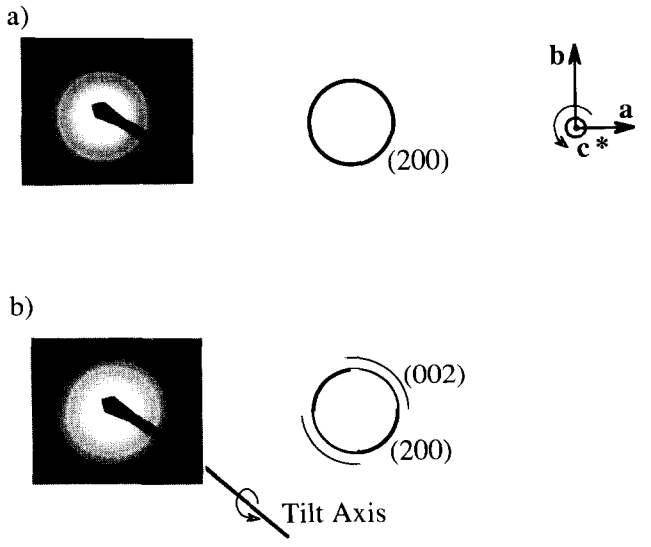

Figure 6 Electron diffraction patterns of a 0.15 μm polyamide-6 film: (a) with normal incidence of the electron beam to the film surface, (b) after a 45 tilt: ***a*** and ***b*** are direct lattice vectors, while c^* is the reciprocal lattice vector

comprises randomly oriented individual lamellae embedded in amorphous material (*Figure 5*). These features will be discussed in more detail below.

The electron-transparent films were also used to determine the crystal structure and the orientation of the crystals. *Figure 6a* is the diffraction pattern obtained with normal incidence of the electron beam of approximately 20 μm diameter sampling a number of discoids in a 0.15 μm thick film. *Table 2* summarizes the indexing of the sharp rings to the corresponding d spacings and crystalline planes. Other than the absence of (0 0 2) diffraction, the pattern matches that of the α form of polyamide-6. *Figure 6b* is the diffraction pattern from the same sample with a tilt of 45°. The rings of *Figure 6a* turn into arcs and a new set of arcs appears after tilting. The rings are formed by the diffraction from the (0 0 2) planes of α-polyamide-6. The absence of (0 0 2) diffraction with normal incidence and formation of arcs after tilting are indications of a preferred orientation in this thin film.

More detailed information on the crystallographic orientation in the films was obtained from X-ray diffraction measurements. *Figure 7* is an example of a series of $2\theta/\theta$ scans for the 1 μm thick film, obtained at various δ angles as described in the 'Experimental'

Table 2 Crystallographic interplanar spacings of α-polyamide-6

(*h k l*)	*d* (Å)
0 1 4 0	1.23
0 0 2	3.70
2 0 0	4.42

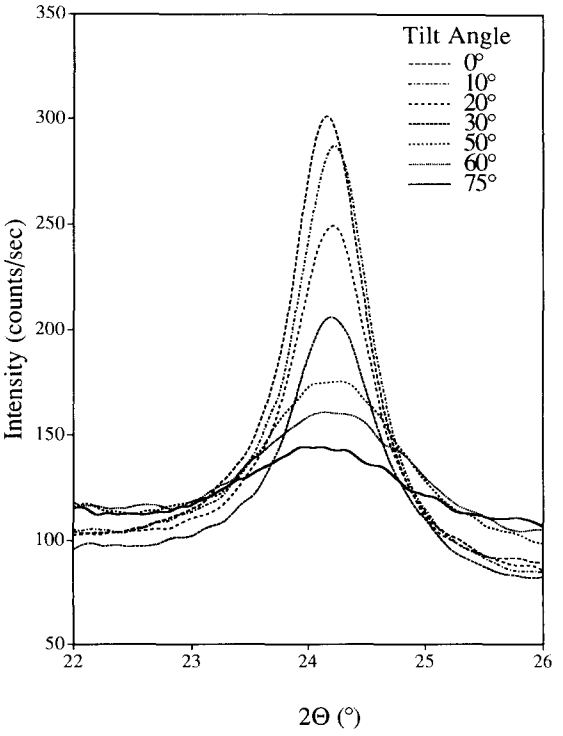

Figure 7 The $2\theta/\theta$ scans of a 2.37 μm thick polyamide-6 thin film at various values of the tilt angle δ. The curves are overlaid to show the variations in the background intensity at various δ angles

section. *Figure 8* shows these same scans in a corrected and shifted form. The correction is necessary to account for changes in the scattering volume and absorption in the thin films as the tilt angle δ is varied from 0° to 75°. In organic materials such as polyamides, X-ray absorption is very low and can be neglected; however, the scattering volume changes considerably with tilt angle. To account for this change, the background signal of each curve was normalized to the background level of the untilted film. In *Figure 7*, the background can be identified to lie in the range of 2θ from 22° to 23° and from 25.2° to 26° for all δ angle values. The weighted average of the normalization factors for all data points in these ranges of 2θ background was used to shift each curve to a common background level. The result of this shift is depicted in *Figure 8*, where the backgrounds are matched and the peak intensities are slightly changed relative to *Figure 7*.

To determine the relative orientation of these (0 0 2) poles, the integral of the corrected X-ray intensity with respect to 2θ from 22° to 26° was calculated. The background was determined by least-squares fitting of a line through the points in the 2θ range of 22–23° and 25.2–26°. The integral of the background curve was then subtracted from the integrated X-ray intensity of the original curves. The resulting integrated intensities of the peaks were normalized with respect to that of the curve at $\delta = 0°$. *Figure 9* is a collective representation of these curves for films of polyamide-6 with different thicknesses. In this figure the curves represent the normalized diffracted intensity of (0 0 2) planes making an angle of δ with the surface. The crystalline orientation should be axisymmetric in the plane of the film owing to the two-dimensional constraint imposed by the thin-film

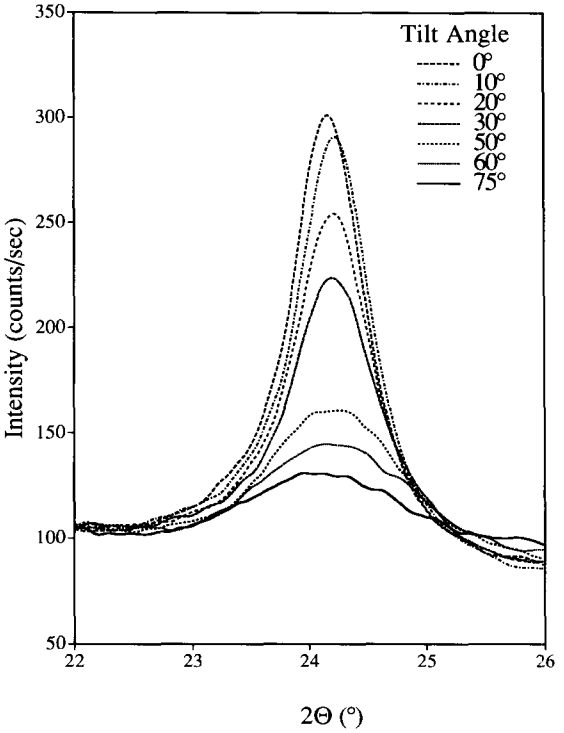

Figure 8 The $2\theta/\theta$ scans shown in *Figure 7* are shown after being shifted by the normalization of the backgrounds to the background of the curve at $\delta = 0$, i.e. the untilted film

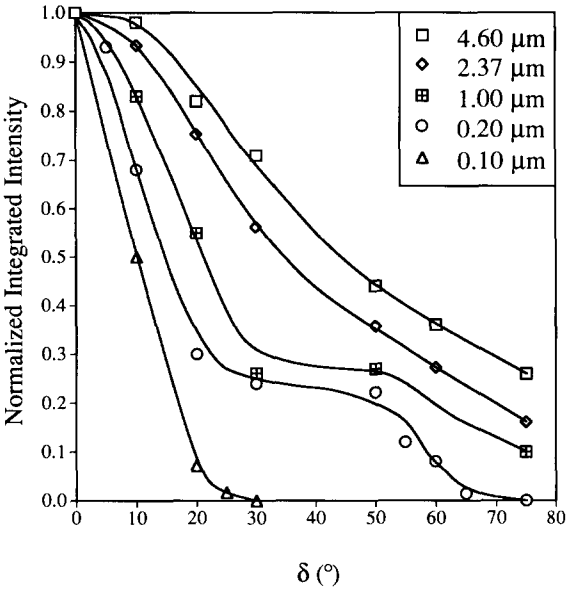

Figure 9 The normalized intensity of the (0 0 2) peak in various thin films of polyamide as a function of tilt angle δ

Table 3 Mechanical properties of thin films of polyamide-6

Film thickness (μm)	Flow stress (MPa)	Apparent Young's modulus (MPa)
0.15 ± 5%	112.5 ± 8.0%	377 ± 7.0%
0.20 ± 6.0%	96.1 ± 3.0%	326 ± 4.0%
1.00 ± 6.0%	63.1 ± 6.0%	133 ± 7.0%
2.15 ± 5.0%	53.4 ± 5.0%	180 ± 10%

geometry. In fact, the Debye–Scherrer rings present in the electron diffraction of *Figure 6a* from a thin film suggest an axisymmetric orientation about the film normal. Therefore, curves identical to those shown in *Figure 9* are expected for every azimuthal β angle, and full pole figures of (0 0 2) planes can be constructed based on this axial symmetry. *Figures 10a–e* show such constructed pole figures for various thin films of polyamide-6. These sombrero-shaped surfaces are three-dimensional representations of the (0 0 2) pole densities, where the z axis is the intensity of the pole at a specific set of Euler angles δ and β.

The results of the uniaxial tensile tests at a strain rate of around $10^{-2}\,s^{-1}$ are displayed in *Figure 11*. The flow stress and the apparent Young's modulus obtained from the linear initial portions of the stress–strain curves decrease with increasing thickness. *Table 3* summarizes these apparent Young's moduli and flow stresses of various thin films. The fracture strains are not clearly defined in these samples, since they tend to tear gradually after the onset of flow. Once tearing initiates, the cross-sectional area decreases and the load drops. Stress and strain plots (load–extension) have little meaning after tearing. Thus, the curves are shown only up to the point where tearing begins. Only the sample of 1.00 μm thickness went to very large uniform strains without tearing.

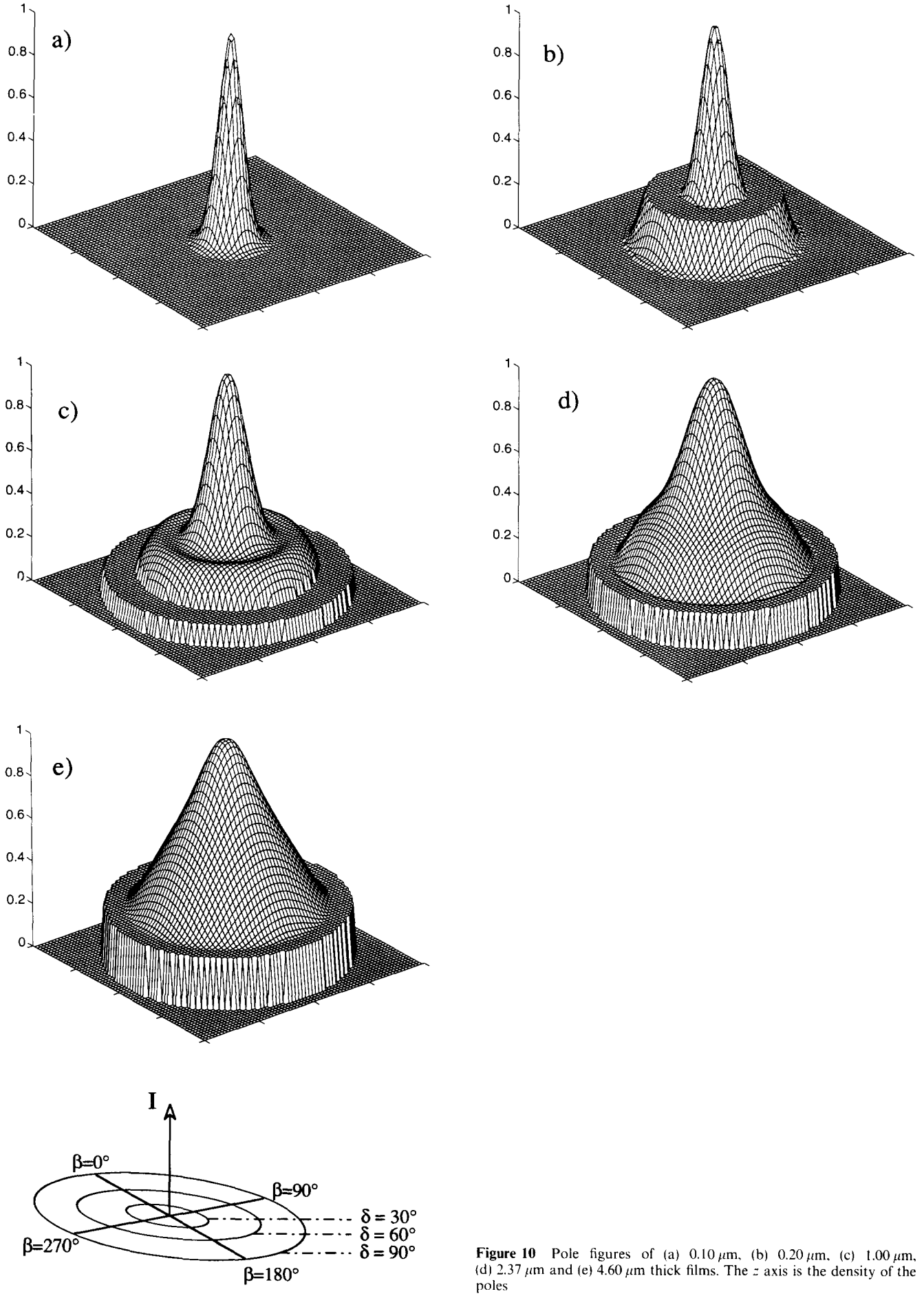

Figure 10 Pole figures of (a) 0.10 μm, (b) 0.20 μm, (c) 1.00 μm, (d) 2.37 μm and (e) 4.60 μm thick films. The z axis is the density of the poles

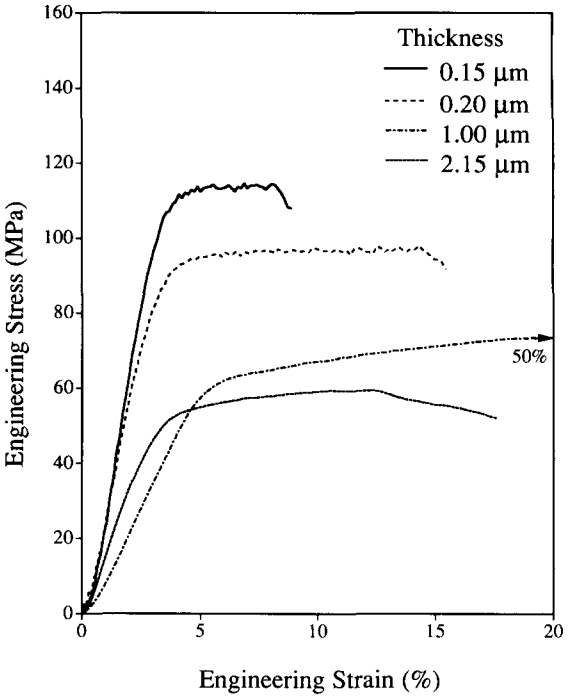

Figure 11 The engineering stress vs. engineering strain of free-standing thin films of polyamide-6 crystallized between polystyrene layers. The strain rate for these samples was in the range of $10^{-2}\,s^{-1}$

DISCUSSION

Crystallites in thin films: TEM study

Grubb[15] has reviewed the effect of radiation on polymers under electron-beam irradiation (TEM), demonstrating that the contrast in thin films of semicrystalline polymers appears after some radiation damage has occurred. This phenomenon was encountered in the polyamide-6 thin films and is the source of the contrast shown in *Figures 4* and *5*. Thus, the morphological features were visible without staining. The crystals first appear as black shadows under the beam. In 3–4 s, the radiation damage destroys the crystalline phase and induces a gradient of mass thickness between the lamellae and the amorphous regions. The destruction of the crystals can be ascertained from the electron diffraction pattern, which transforms itself from a collection of sharp rings to a diffuse pattern during the same time-frame as the contrast build-up occurs. According to Grubb[15], the crystalline regions distort upon radiation damage; this, in turn, results in an undulated thin film with increasing surface relief where the destroyed crystals are thicker and the amorphous regions are now thinner. The mass thickness variation throughout the film is thought to provide the contrast.

Studies on the crystalline morphology of bulk semicrystalline polymers have shown that lamellae organize themselves into a spherulitic structure[16]. It is also known that, under certain geometric constraints, semicrystalline polymers are not capable of growing three-dimensional spherulites[11–14,17–20]. For instance, Phillips and Vatansever[19] have prepared solution-cast thin films of *cis*-polyisoprene to study the crystallization regime transitions. Their films crystallized in a spherulitic structure with an in-plane diameter (2.5 μm) about 3 times larger than the film thickness (800 Å), suggesting two-dimensional crystalline aggregates. Similarly, theoretical calculations have shown that, in thin films, the lamellae are arranged in rather disc-shaped crystalline aggregates[18]. The TEM results of the present study support such constraint effects. *Figure 4* shows a TEM micrograph of a polyamide-6 thin film crystallized between two layers of PS. The film is 0.15 μm thick, while the average lateral dimension of a crystal aggregate is around 1.25 μm. Considering the thickness of the film and the diameter of the crystal aggregate, it is reasonable to conclude that these crystal aggregates have a 'discoid' structure. Based on such TEM observations the following model, illustrated in *Figure 12*, is proposed for the organization of the lamellae in the polyamide-6 thin film. The growth of the lamellae is constrained by the confined film geometry and is only free in the plane of the film. Consequently, lamellae nucleated from the same point eventually organize into a disc-shaped crystal. *Figure 12* has been drawn with chain axis ***b*** in the plane of the film for reasons that will be explained below.

Another interesting aspect of this morphology lies in the inter-discoid region: unlike bulk spherulitic morphologies, in which spherulite impingement occurs, many of the discoids did not impinge on each other in the thin films. These inter-discoid regions are also semicrystalline with well defined lamellae, which are, however, organized randomly. Although the radiation damage is advantageous in sharpening the contrast, it is not so in recording the electron diffraction patterns. Before the crystals are destroyed, the diffraction pattern is composed of sharp rings, which become diffuse as the radiation damage progresses. However, one can tilt the sample and observe arcs in the diffraction pattern for a few seconds before radiation damage occurs. In order to carry out a detailed analysis of these rings to determine

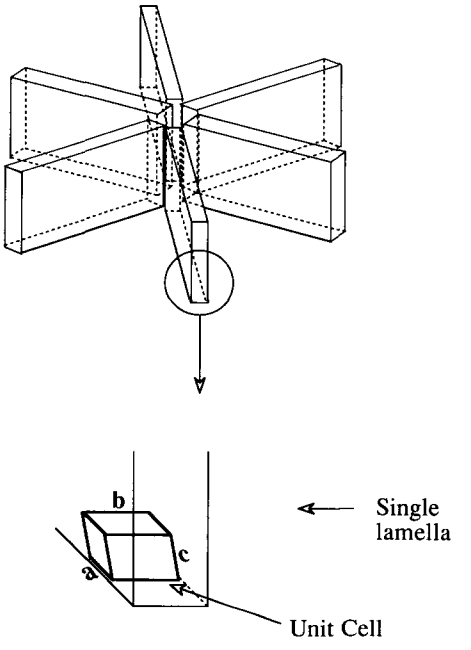

Figure 12 The proposed model showing the organization of the lamellae in a very thin film of polyamide-6. The disc shape of the crystal is justified by TEM observations. The X-ray results showed that the chain axis is parallel to the interface

the crystal structure and orientation, the TEM was operated at a lower accelerating voltage of 100 kV. This provided enough time to record the diffraction pattern on a photographic plate before the radiation damage occurred. *Figure 6a* is the diffraction pattern of a 0.15 μm film with normal incidence of the electron beam. The rings represent various d spacings of the direct lattice. By using an internal TlCl standard of known d spacing, the d spacings for each ring of *Figure 6a* were calculated (see *Table 2*). These d spacings correspond to the α crystal form of polyamide-6 and are identical for films of various thicknesses, indicating no influence of film thickness on crystal structure. The α form of polyamide-6 is monoclinic and belongs to the $P2_1$ space group, for which the diffraction is absent for $l=2n+1$ for the family of (0l0) planes. The chain direction and the screw axis 2_1 are parallel to the $\boldsymbol{b}$ axis. The lattice parameters are $a=9.56$ Å, $b=17.24$ Å and $c=8.01$ Å with $\beta=67.5°$. There are eight monomer units per unit cell. The diffraction pattern of *Figure 6a* represents the reciprocal lattice: the inner ring is from the (2 0 0) planes and the outer ring is from the (0 14 0) planes. The absence of diffraction spots or arcs in *Figure 6a* suggests a random orientation of the crystals in the plane of observation; however, the (0 0 2) ring representing the hydrogen-bonded planes is absent. This is due to a preferred orientation of (0 0 2) planes such that the diffraction condition from these planes is not satisfied[13]. One way of determining the existence of preferred orientation is to tilt the sample about an axis and examine the changes in the diffraction pattern. *Figure 6b* is recorded after a tilt of 45°. The existing rings transform into arcs after tilting and a new diffraction appears from a spacing of 3.70 Å, which corresponds to hydrogen-bonded sheets in the (0 0 2) planes. This indicates a preferred orientation of the hydrogen-bonded planes parallel to the surface of the thin film: that is, the reciprocal lattice vector $\boldsymbol{c}^*$, which is normal to (0 0 2) planes, is also normal to the film surface, while direct lattice vectors $\boldsymbol{a}$ and $\boldsymbol{b}$ assume random directions in the plane of the film. It is rather difficult to quantify this orientation using electron diffraction owing to rapid radiation damage and low transmission of electrons through thick films. Therefore, X-ray pole figure measurements were conducted to determine the orientation as a function of film thickness in a more quantitative measure.

Influence of thickness on crystalline orientation: X-ray study

As explained above, the crystalline orientation could not be determined from electron diffraction experiments owing to rapid radiation damage. Instead, X-ray diffraction was used to study changes in the orientation of the polyamide-6 crystals as the film thickness was varied from 0.10 to 4.60 μm. The films were mounted on a pole figure attachment and a series of $2\theta/\theta$ scans were performed at various tilt angles δ. A $2\theta/\theta$ scan detects only the planes that are parallel to the surface of the film. When the sample is tilted by δ, only the diffraction from the planes that are inclined at an angle δ to the surface are detected. After correcting for changes in the scattering volume, one can obtain a 'partial' pole figure, representative of the texture in the film. *Figure 9* summarizes these results. The y axis represents the density of (0 0 2) poles and the x axis is the tilt angle between the normal of the thin film and the (0 0 2) plane normal, i.e. reciprocal lattice vector $\boldsymbol{c}^*$. For the 0.10 μm film, most of the (0 0 2) planes are either parallel to the surface or are tilted up to 25°, whereas the 4.60 μm film has (0 0 2) planes in every orientation with a decrease in intensity as the tilt angle increases to 75°.

A clearer way of presenting the data of *Figure 9* is to construct full pole figures. The orientation of the crystalline planes is axisymmetric in the plane of the films, as confirmed by the rings of the electron diffraction pattern in *Figure 6*. Consequently, the curves in *Figure 9*, which are measured at the Euler angle $\beta=0°$, are identical for every β angle. Therefore, full pole figures can be constructed by rotating the curves of *Figure 9* around the y axis. The results are illustrated in *Figures 10a–e* where the z axis is the density of the (0 0 2) poles. These 3D orientation distributions indicate that the sharp peak of the 0.10 μm film reflects a clustering of (0 0 2) planes parallel to the surface of the film. For the slightly thicker 0.20 μm film, the sharp peak is still present; however, a new family of planes starts to emerge. The intensity of this new family of planes increases with increasing thickness until the sharp peak disappears in the film of 2.37 μm thickness. For thicker films the density of poles increases and a cone-shaped surface is formed. Eventually, for a perfectly random sample the surface would assume a cylindrical shape indicating a uniform distribution of (0 0 2) pole density.

This orientation study reveals that, in thin films of polyamide-6, (0 0 2) planes are preferentially oriented parallel to the initial rubber interface (the subsequent free surfaces) with a random azimuthal orientation. For thicker films, the orientation distribution approaches that of bulk polyamide-6. The preferred orientation of hydrogen-bonded sheets parallel to the film plane arises in other polyamides as well. Keller[13] and Scott[14] have independently shown that thin films of polyamide-6,6 experience a similar orientation in which the (0 1 0) crystallographic planes containing hydrogen-bonded sheets remain in the plane of the film. Polyamide-6,10 assumes a similar orientation in thin-film geometries[13].

The high anisotropy of polyamide crystals can account for the orientation of hydrogen bonding in the plane of thin films: in a polyamide crystal, chains are attached with strong hydrogen bonds that arrange in sheets, which interact with relatively weak van der Waals forces. The relative difference between the energies of these secondary forces results in a high anisotropy in terms of surface energies of the crystal. It is therefore very likely for polyamides to align the low-energy hydrogen-bonded planes preferentially parallel to the rubber or glass interfaces to minimize the interfacial free energy. Such a phenomenon has been observed in other systems: for instance, a thin film of tin on a PS film assumes a perfect orientation of (0 0 1) planes parallel to the interface[10]. Similarly, in thin films of lamellar block copolymers of poly(styrene-*block*-methyl methacrylate) (P(S-b-MMA)) an alternating assembly of PS and PMMA blocks forms upon annealing with the lamellae oriented parallel to the interface[21]. The effect of the interface on these systems seems to decline in thicker films. In both the Sn/PS and block copolymer systems the preferred orientation comes about from the minimization of the interfacial free energy by creating low-energy contacts with the substrate.

As shown above, the preferred orientation in thin

films of polyamide-6 degenerates as the film thickness increases, i.e. as the two rubber/polyamide interfaces move apart. In fact, an oriented skin layer should always be present near the interface. When the film is thin, the interfaces are close to each other and the skin layers overlap, leaving the whole film with a preferred orientation. As the film thickness increases and the interfaces move apart, at a critical film thickness ($\sim 0.07\ \mu m$), the skin layers cease to overlap. This results in the appearance of increasing thicknesses of randomly oriented material in the bulk of the film. It is important to note that in polyamide-6 the (0 0 2) planes are parallel to the chain axis [0 2 0]. This indicates that the chain axis is parallel to the surface of the film. That is, during crystallization, a chain segment prefers to lie parallel to the film surface near the interface. The outcome of the orientation measurements supports the sketch of *Figure 10* where the chain direction ***b*** is drawn in the plane of the film.

Mechanical properties of thin films: Instron study

Semicrystalline polymers are composites, which, when in organized form, consist of the alternating organization of crystalline and amorphous layers. The mechanical properties of these building blocks define the macroscopic behaviour of the polymer under various states of stress. While amorphous regions have more or less isotropic properties, the crystalline regions are strongly anisotropic. Therefore, the overall crystalline orientation affects the mechanical properties of the polymer. Slip, the main mode of inelastic deformation in the crystalline component of the semicrystalline polymers, encounters various levels of resistance depending upon the type of slip plane and its geometrical relation relative to the applied stress axis. Lin and Argon[22] have shown that three slip systems can be activated in polyamide-6, namely the (0 0 1)[0 1 0] and (1 0 0)[0 1 0] chain slip systems and the (0 0 1)[1 0 0] transverse slip system. The corresponding critical resolved shear stresses (*CRSS*) are reported to be 16.24, 23.23 and 23.18 MPa respectively at room temperature. The (0 0 1)[0 1 0] chain slip is easier to activate than the other slip systems. As determined above, in the thin films of polyamide-6, the crystallite orientation relative to the film surfaces depends strongly on film thickness. Therefore, the mechanical properties should also depend on the thickness. *Figure 11* clearly demonstrates this effect — the flow stress and the apparent modulus decrease with increasing film thickness. For the $0.15\ \mu m$ thick film, the (0 0 2) planes are observed to be parallel to the surface of the film. At this orientation the resolved shear stress on these (0 0 2) planes is nearly zero and slip initially occurs on the other high-resistance slip systems. This increases the flow stress considerably and the film yields at 108 MPa. In comparison, the $2.15\ \mu m$ thick film consists of both oriented skin layers and a substantial amount of randomly oriented core region. In this case, the resolved shear stress on most of the (0 0 2) planes is finite. This in turn leads to a decrease in the macroscopic flow stress, as the thickest film yields at 48 MPa. The changes in the apparent modulus are also due to changes in the orientation distribution. These effects can be quantitatively modelled by means of polycrystal plasticity models of the type described by Lee *et al.*[23], and modified for use with polyamide-6 by Ahzi *et al.*[24]. These models are presently being used to elucidate different mechanical behaviours of these films; the results will be published in due course.

Local orientation in the proximity of second-phase particles in a filled polyamide-6

The present study lends strong support to the view that, in a rubber/polyamide-6 blend, the (0 0 2) planes of polyamide-6 are preferentially aligned parallel to the interfaces. Therefore, in a rubber-modified polyamide-6 the local crystalline orientation of the matrix in the proximity of a rubber particle could be altered, resulting in a locally oriented skin layer around the interface. If the interparticle distance is small, the skin layers would overlap, resulting in a locally oriented interparticle region. For a sparse distribution of the particles, the overlap will be minimal. Under these conditions, the orientation of the matrix would be randomized.

In a rubber-modified polyamide where the particles are closely spaced, the locally oriented interparticle regions would possess a high degree of anisotropy. As a result, the local flow stress will vary depending on the relative direction of the applied stress. When the resolved shear stress on the (0 0 2) planes of the oriented interparticle region is high, the flow stress in these regions will be reduced markedly. As long as such regions percolate through the specimen, the overall flow stress will be reduced. As a consequence, early precipitation of fracture processes will be avoided and the specimen will have a high strain to fracture; hence the blend would be tough. Since the overlap of the skin layers would occur at a critical interparticle distance, the above mechanism of toughening is consistent with Wu's observation of a critical interparticle distance for a brittle-to-tough transition[25]. Preliminary studies in our laboratory on ethylene–propylene–diene rubber-modified polyamide-6,6 support these assertions. The results of these studies will be the subject of a forthcoming paper.

CONCLUSIONS

Crystallization of polyamide-6 in the form of thin films on a PS- or EPDR-coated silicon substrate produces lamellae organized into a disc-shaped crystal aggregate, namely a 'discoid'. The transition from discoids to spherulites occurs at a film thickness of about $2\ \mu m$. Below this critical limit the diameters of the crystal aggregates are larger than the thickness of the film; and above $2\ \mu m$ thickness the crystal aggregate size is smaller than the film thickness. From the electron and X-ray diffraction studies, it follows that polyamide-6 prefers to have its low-energy (0 0 2) hydrogen-bonded planes parallel to a rubber interface. This gives rise to a preferred orientation within a skin layer of $0.07\ \mu m$ in thin polyamide films. For film thicknesses below $0.15\ \mu m$, these oriented skin regions overlap and the film has a preferred orientation as a whole. Thicker films lead to a random orientation of crystals since the influence of the interface cannot penetrate more than $0.05–0.07\ \mu m$. The dependence of the orientation of (0 0 2) planes on thickness affects the mechanical properties of thin films: the Young's modulus and flow stress both drop with increasing thickness. This observation is in accord with the crystallographic texture of the films and the known slip resistances of the polyamide-6 crystal. Finally, the morphology–property

relations observed for these thin films of polyamide-6 are thought to have relevance to the mechanism of modification of polyamide-6 via second-phase particles.

ACKNOWLEDGEMENTS

This research was supported by NSF/MRL, through the Center for Materials Science and Engineering at MIT under Grant No. DMR-90-22933 and by a DuPont Graduate Fellowship for OKM, for which we are grateful to Dr D. Huang of the DuPont Co.

REFERENCES

1 Mai, Y. W. and Williams, J. G. *J. Mater. Sci.* 1977, **12**, 1376
2 Flexman, E. A. *J. Polym. Eng. Sci.* 1979, **19**, 564
3 Wu, S. *Polymer* 1985, **26**, 1855
4 Borggreve, R. J. M., Gaymans, R. J., Schuijer, J. and Ingen-Housz, J. F. *Polymer* 1987, **28**, 1489
5 Shiao, M. L., Nair, S. V., Garrett, P. D. and Pollard, R. E. *Polymer* 1994, **35**, 306
6 Wyzgoski, M. G., Novak, G. E. and Simon, D. L. *J. Mater. Sci.* 1991, **26**, 6314
7 Kumamaru, K., Oono, T., Kajiyama, T. and Takayanagi, M. *Polym. Compos.* 1983, **4**, 141
8 Yu, Z., Ait-Kadi, A. and Brisson, J. *Polymer* 1994, **35**, 1409
9 Kojima, Y., Usuki, A., Kawasumi, M., Okada, A., Kurauchi, T., Kamigaito, O. and Kaji, K. *J. Polym. Sci. (B) Polym. Phys.* 1994, **32**, 625
10 Reffner, J. R. PhD thesis, University of Massachusetts at Amherst, 1992
11 Andrews, E. H. *Proc. R. Soc. Lond. (A)* 1963, **277**, 562
12 Andrews, E. H. *Proc. R. Soc. Lond. (A)* 1962, **270**, 232
13 Keller, A. *J. Polym. Sci.* 1959, **35**, 361
14 Scott, R. G. *J. Appl. Phys.* 1957, **28**, 1089
15 Grubb, D. T. *J. Mater. Sci.* 1974, **9**, 1715
16 Bovey, F. A. and Winslow, F. H. 'Macromolecules: An Introduction to Polymer Science', 1st Edn., Academic Press, New York, 1979
17 Billon, N. and Haudin, J. M. *Colloid Polym. Sci.* 1989, **267**, 1064
18 Billon, N., Escleine, J. M. and Haudin, J. M. *Colloid Polym. Sci.* 1989, **267**, 668
19 Phillips, P. J. and Vatansever, N. *Macromolecules* 1987, **20**, 2138
20 Andrews, E. H., Owen, P. J. and Singh, A. *Proc. R. Soc. Lond. (A)* 1971, **324**, 79
21 Mayes, A. M., Russell, T. P., Satija, S. K. and Majkrzak, C. F. *Macromolecules* 1992, **25**, 6523
22 Lin, L. and Argon, A. S. *Macromolecules* 1992, **25**, 4011
23 Lee, B. J., Argon, A. S., Parks, D. M., Ahzi, S. and Bartczak, Z. *Polymer* 1993, **34**, 3555
24 Ahzi, S., Lee, B. J. and Asaro, R. J. *J. Mater. Sci. Eng.* submitted for publication
25 Wu, S. *J. Appl. Polym. Sci.* 1988, **35**, 549